

Killing Two Birds with One Stone: Biomineralized Bacteria Tolerate Adverse Environments and Absorb Hexavalent Chromium

Rongbing Tang,[§] Liheng Shen,[§] Lu Yang, Kai You, Zhihui Li, Xiaorui Wei, and Jing Wang*Cite This: *ACS Omega* 2022, 7, 15385–15395

Read Online

ACCESS |



Metrics & More

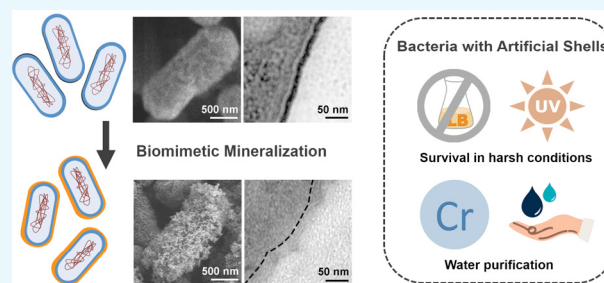


Article Recommendations



Supporting Information

ABSTRACT: Heavy metal ions in contaminated water, such as hexavalent chromium, are harmful to humans. Bacterial biosorption is an ideal method for the treatment of hexavalent chromium. However, hexavalent chromium in solution causes bacteria to produce reactive oxygen species, which leads to bacterial death and affects biosorption. We developed a microfluidics-based biomimetic mineralization method to encapsulate bacteria (e.g., *Escherichia coli* and *Bacillus subtilis*) with zeolitic imidazolate framework-8 (ZIF-8), thus allowing the bacteria to form a continuous and homogeneous shell. The artificial shells endowed bacteria with the ability to tolerate harsh environments, which was significant during the treatment of contaminated water. The adsorption of hexavalent chromium was a two-step process: first the fast physical adsorption of ZIF-8 and biosorption by bacteria (up to 30–50% adsorption in 1 day), followed by secondary biosorption after decomposition of the system. The maximum adsorption of hexavalent chromium by the encapsulated bacteria reached 90%. The microfluidic device developed in this study provides a simple method to encapsulate bacteria mildly and enable cell survival in extreme environments, offering the possibility of future microbial applications in environmental and other fields.



1. INTRODUCTION

Chromium-containing chemicals are used in a wide range of industrial processes, such as leather tanning, mining operations, alloy, paint and pigments, glass industry, wood preservation, film, and photography.^{1–3} Hexavalent chromium is an environmental pollutant and a recognized carcinogen.^{1,4} Cr (VI) exhibits high toxicity and causes diarrhea, ulcers, eye and skin irritation, and, in severe cases, even renal insufficiency and lung cancer.^{5,6} Chromium-contaminated wastewater puts pressure on the environment, so various techniques have been employed to treat Cr(VI)-contaminated water, such as physical adsorption, electrochemical precipitation, ion exchange, ultrafiltration, and reverse osmosis. However, there are many major drawbacks involved in the pre- and post-treatment of wastewater, including high cost, complex process, low removal efficiency, and even secondary contamination.^{7–10}

Biosorption is a promising technology for the removal of hexavalent chromium from wastewater, which is economical, efficient, and environmentally friendly.^{4,11–13} Organisms including bacteria, fungi, yeast, algae, and plants have shown the ability to remediate.^{2,14–16} However, the poor resistance of bacteria to contaminants is a bottleneck for biotechnology application.^{3,13} Hexavalent chromium has good cell membrane permeability and readily enters bacteria, where it subsequently undergoes reduction reactions and generates free radicals (e.g., reactive oxygen species), leading to bacterial death.^{2,4} Bacteria with resistance to hexavalent chromium are usually isolated from contaminated soil and water for further use in the

biosorption.^{15,17} The isolation and culture of specific bacteria is complex and difficult.^{15,17} Therefore, we hope that, by improving the tolerance of common bacteria to extreme environments, common bacteria can also be applied to biosorption. In recent years, researchers found that bacteria could be modified by inorganic nanoparticles, polymers, and metal–organic frameworks (MOFs) to enhance their resistance to harsh environments.^{18–22} MOFs are synthesized by cross-linking metal ions/clusters with organic linkers. Their intrinsic porous properties, abundant functionalities as well as exceptional thermal and chemical stabilities have led to a wide range of applications, such as gas separation and adsorption, catalysis, treatment of pollutants, and biomineralization.^{23–27} Among MOF materials, zeolitic imidazolate framework-8 (ZIF-8) is one of the most popular candidates in biomineralization, due to the mild synthetic conditions and excellent biocompatibility.^{23–25,28} Liang and co-workers demonstrated that ZIF-8 could be used to modify the surface of *Saccharomyces cerevisiae*.²⁹ In this way, the living yeast cells could live in

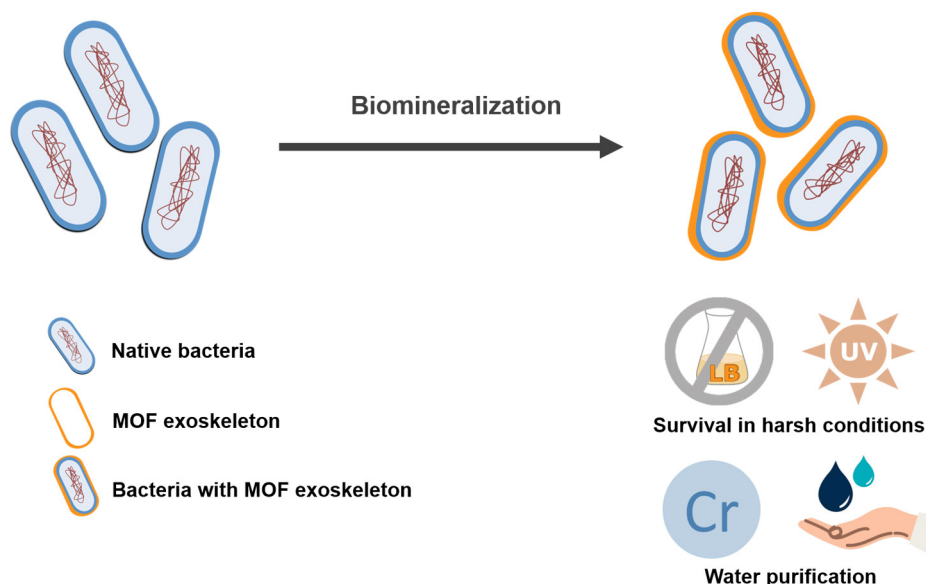
Received: December 5, 2021

Accepted: April 15, 2022

Published: April 27, 2022



Scheme 1. Biomining of Bacteria Based on Microfluidics for Water Purification



harsh conditions and restore growth vitality as before with the removal of the shell.²⁹

Escherichia coli (*E. coli*) and *Bacillus subtilis* are common Gram-negative and Gram-positive bacteria with protein-rich surfaces that can serve as ligands and pro-nucleosomes for metal ion reactions. Herein, we propose a microfluidic approach to achieve biomining of common bacterial surfaces with ZIF-8 for better protection of bacteria and water purification (Scheme 1). We refer to the encapsulated *Escherichia coli* and *Bacillus subtilis* as *Escherichia coli*@ZIF-8 (*E. coli*@ZIF-8) and *Bacillus subtilis*@ZIF-8, respectively. The device we designed consists of a dual-channel microinjection pump, connection system, and receiver, which was connected by polytetrafluoroethylene tubes and luer joints for stable delivery of ligands and metal ion fluids through laminar rather than turbulent flow. The modified technique based on microfluidics allows for more precise control of the reaction and a more uniform shell on the surface of the bacteria, which achieves better protection of the bacteria and ultimately the physical and biological uptake of Cr(VI) from contaminated water.

2. MATERIALS AND METHODS

2.1. Materials. Zinc acetate dihydrate ($\text{Zn}(\text{CH}_3\text{COO})_2 \cdot 2\text{H}_2\text{O}$), 2-methylimidazole (2MI), Sodium dichromate ($\text{Na}_2\text{Cr}_2\text{O}_7 \cdot 2\text{H}_2\text{O}$), ethanol, acetone, and glutaraldehyde were purchased from Sinopharm Chemical Reagents Co., Ltd. (Shanghai, China). Phosphate buffer saline (PBS) was produced by Thermo Fisher Scientific Co., Ltd. (Shanghai, China). The Luria–Bertani broth was obtained from Solarbio Science & Technology Co., Ltd. (Beijing, China). Bull serum albumin–Rhodamine B isothiocyanate (BSA–RBITC) was purchased from Beijing Bioss Biotechnology Co., Ltd. (Beijing, China). EDTA solution (0.5 M, pH 8.0) and a reactive oxygen species (ROS) assay kit were purchased from Shanghai Beyotime Technologies Inc. (Shanghai, China). Fluorescein diacetate (FDA) and propidium iodide (PI) double staining cell viability assay kit was from Shanghai BestBio Biotechnology Co., Ltd. (Shanghai, China).

2.2. Cell Culturing and Harvesting. *Escherichia coli* (*E. coli*, ATCC 25922) and *Bacillus subtilis* (ATCC 6051) were provided by the Center for Microbial Preservation, School of Stomatology, Lanzhou University, China. The transgenic *E. coli* with green fluorescent protein was purchased from Fenghui Biotechnology Co., Hunan, China. The lyophilized powder of transgenic *E. coli* was dissolved in lysis solution and transferred to Luria–Bertani (LB) agar plates. Frozen *E. coli* and *Bacillus subtilis* were grown overnight at 37 °C on the LB agar plates. The agar plates of bacteria should be kept for less than one month. Individual colonies of *E. coli*, transgenic *E. coli*, or *Bacillus subtilis* were transferred to LB broth (10 g of peptone, 10 g of NaCl, and 5 g of yeast extract in 1000 mL of H_2O) in a shaking incubator at 37 °C overnight. When the optical density (OD) of the liquid at 600 nm was around 0.5, *E. coli* were harvested and washed three times by PBS. The white pellet obtained after centrifugation was used immediately for further experiments.

2.3. Construction of the Microfluidic Device. A dual-channel microsyringe pump (LSP02-1B, Lange, Baoding, China) was connected to syringes to precisely control the flow rate of the two precursor fluids, as shown in Figure S2. The syringes mounted on the dual-channel microsyringe pump were connected to the receiver via polytetrafluoroethylene (PTFE) tubes and luer fittings. The microfluidic receiver was designed by Auto Computer-Aided Design (Autodesk, Inc., San Rafael, CA) and produced by a 3D printer (ENDER-5S, Creative 3D, Shenzhen, China). There were grooves on the inner wall of the cylindrical receiver that allowed the PTFE tube to be placed spirally. The radius of the spiral was 45 mm, and the spacing of the spiral was 10 mm. The bottom surface of the receiver was circular, and the ultrasonic probe (JY88-IIN, ACIENTZ, Ningbo, China) was placed in the center of the circle.

2.4. Encapsulation of *Escherichia coli* by a General Method. First, active *E. coli* were cultured to logarithmic growth phase and resuspended in 1 mL of 2MI (160 mM) and gently stirred at room temperature. Subsequently, the solution became instantly whitish when one milliliter of zinc acetate (40 mM) was rapidly added. The solution was then stirred at 300

rpm for 10 min for adequate biomimetic mineralization.²⁹ The resulting opaque solution was then centrifuged at 5000g for 5 min and washed three times with deionized water. Finally, the white pellet of biomimetic mineralized *E. coli* was obtained and dispersed in 1 mL of deionized water.

2.5. Encapsulation of *Escherichia coli* by Microfluidic Device. First, active *E. coli* were resuspended in 1 mL of 2MI (160 mM) and gently stirred at room temperature. Subsequently, 1 mL of zinc acetate (40 mM) was added rapidly at 1000 $\mu\text{L}/\text{min}$ using a micro syringe pump and sonicated for 10 min (150 W, 20 ± 0.5 kHz). The resulting opaque solution was then centrifuged and washed three times with deionized water. Finally, the white particles obtained after centrifugation were dispersed in 1 mL of deionized water.

2.6. Characterization of Encapsulated *E. coli*. X-ray photoelectron spectra (XPS) patterns were collected from Kratos AXIS Ultra DLD equipment. X-ray diffraction (XRD) patterns were received from a Rigaku D/Max-2400 (Cu target, $\lambda = 1.542 \text{ \AA}$, 45 kV, 200 mA). The synthesis of MOF exoskeleton of encapsulated *E. coli* was confirmed by Fourier transformed infrared (FTIR) spectroscopy analysis, and the FTIR spectra of the samples were recorded on a Nicolet Nexus 670 spectrophotometer. The encapsulated bacteria were observed under a confocal laser scanning microscope (CLSM, Olympus Fluoview 3000). The morphology and microstructure characterization of encapsulated *E. coli* were carried out on a scanning electron microscope (SEM, HITACHI SU8100) and transmission electron microscope (TEM, HITACHI HT7800, FEI Tecnai F30). Element composition and distribution were utilized by an energy dispersive spectrometer (JEOL FJSM-5600LV) and element mapping was by a Bruker XFlash Detector.

2.7. Colocalization of *Escherichia coli*@ZIF-8. Transgenic *E. coli* were observed by a confocal laser scanning microscope (CLSM) to emit green fluorescence. The cell shell ZIF-8 was labeled with BSA-RBITC during the mimic mineralization and then observed by CLSM. The percentage of encapsulated cells was tested by flow cytometry assay in GFP and RBITC channel on a NovoCyte flow cytometer of Agilent Technologies, Inc.

2.8. Bacterial Viability after Long-Term Storage. The encapsulated and common bacteria were nutrient-deprived for 7 days, and then, cell viability was measured. The encapsulated shell of the bacteria was removed by EDTA, which could be cross-linked with metal cations. One milliliter of EDTA dilution (50 mM) was added to 1 mL of cell suspension and placed in a constant temperature shaking incubator for 10 min. The turbid solution was centrifuged, washed three times with PBS at pH 7.0 to remove residual impurities, and centrifuged to obtain white pellets for further experiments. Growth curve tests were performed on encapsulated *E. coli* after the removal of cell shell and native *E. coli*. Ten microliters of the bacterial broth was dispersed into 30 mL of LB broth and placed in a shaking incubator at 37°C and 200 rpm. The OD_{600} of the cell fluid was measured by a spectrophotometer every 2 h for 24 h.

2.9. Viability of Bacteria under Ultraviolet Light Irradiation. The native and encapsulated bacteria were treated with ultraviolet light (254 nm, $80 \mu\text{W}/\text{cm}^2$) for half an hour. We also tested the power density of UV light using a UV irradiation meter (SDR254, Speedre, Shenzhen, China). We placed the probe at the same location as the bacteria and measured the power density of UV light there after connecting the probe to the host. We found that the UV intensity

remained stable and removed the probe. After half an hour of UV radiation, the encapsulated shell of the bacteria was removed by EDTA. One milliliter of cell fluid was added with 10 μL each of FDA and PI stain, and the mixture was placed in a constant temperature incubator for 30 min. The stained cells were washed three times with PBS to remove residual staining and dispersed in 1 mL of PBS buffer solution. Then, microbial cells were observed under CLSM. The green cells were alive, and the red cells were dead. The ROS produced by the cells were detected by the ROS assay kit and observed by inverted fluorescence microscopy. The intensity of green fluorescence represented the amount of ROS, which was quantified using ImageJ.

2.10. Tolerance to Hexavalent Chromium in Solution. The bacteria were cultured to the growth logarithmic stage with an OD_{600} of 0.5. After biomimetic mineralization, the bacteria were resuspended in an aqueous solution containing 5 mg/L hexavalent chromium for an additional 3 h. After the cell shell was removed with EDTA, the cells were treated with FDA/PI double staining cell viability assay kit and observed with CLSM.

2.11. Absorptive Capacity for Cr(VI) in Solution. The bacteria were cultured to the logarithmic stage of growth with an OD_{600} of 0.5. We took cell cultures of *E. coli* and *Bacillus subtilis* in logarithmic growth phase, respectively, and the solutions were centrifuged and used for the determination of chromium ion concentration uptake capacity. After the biomimetic mineralization on the surface, bacteria were centrifuged at a high speed, washed with deionized water, and resuspended in an aqueous solution containing 5, 25, and 50 mg/L Cr(VI), respectively. After 1, 2, 3, 4, 5, 6, and 7 days, the samples were removed from the cultures. The cell culture solution was passed through a $0.22 \mu\text{m}$ filter and made acidic with concentrated sulfuric acid. The above solution (200 μL) was added with 8 μL of 1,5-diphenylcarbazide (0.2 g in 50 mL of absolute acetone and 50 mL of pure water). The formed purple complexes were analyzed at 540 nm using a UV-vis spectrophotometer (UV2450, Shimadzu Commercial Systems). The standard curve needed to be redrawn with the standard Cr(VI) solution for each experiment, and the Cr(VI) in solution was calculated by the standard curve regression equation.

The percentage of removed hexavalent chromium ions in the solution was calculated using the following equation:

$$\% \text{removal} = \frac{C_0 - C_t}{C_0} \times 100 \quad (1)$$

where C_0 (mg/L) is the initial Cr(VI) concentration, and C_t (mg/L) are the metal concentrations at the equilibrium liquid phase and at any time t . We performed the same determination of the absorption capacity of hexavalent chromium ions for 100 mg of ZIF-8.

2.12. Statistical Analysis. All experiments were arranged in completely randomized designs with three repetitions. When a factor or any interaction between factors was deemed significant, pairwise comparisons were performed using a t test, and corrections for multiple comparisons were performed using Tukey's test. The significance level was set at $p \leq 0.05$.

3. RESULTS AND DISCUSSION

3.1. Preparation of *Escherichia coli*@ZIF-8. The *E. coli*@ZIF-8 obtained by microfluidic methods could survive in harsh

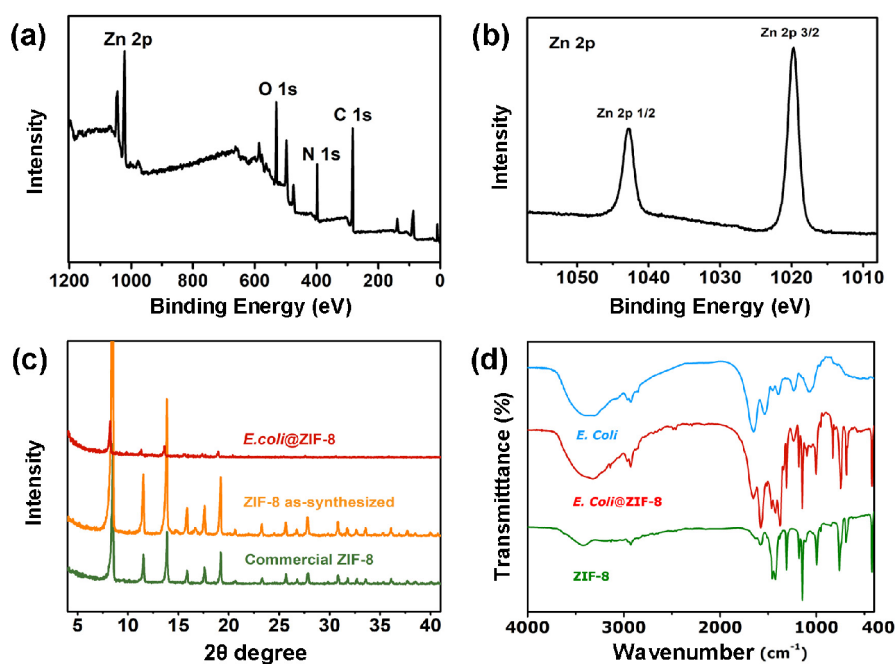


Figure 1. Characterization of MOF exoskeleton. (a) XPS survey spectrum of the *E. coli*@ZIF-8 at room temperature. (b) High-resolution XPS spectra of Zn 2p region. (c) XRD characterization of the *E. coli*@ZIF-8 composites comparing synthesized ZIF-8 and commercial ZIF-8. (d) FTIR spectra of native *E. coli* cells (blue), *E. coli*@ZIF-8 (red), and pure ZIF-8 (green) with wavenumbers of 4000–400 cm^{-1} . All samples were dried in 65 $^{\circ}\text{C}$ ovens for 8 h.

environments and remove heavy metals from polluted water (Scheme 1). The microfluidic device was simple, economical, nontoxic, reusable, and consisted of a two-channel micro-injection pump, a connection system, and a receiver (Figure S2). The receiver was designed by the software of Auto CAD and manufactured by the 3D printer, which was made of poly(lactic acid) (PLA) with excellent biocompatibility.³⁰ The connection system consisted of PTFE tubes and luer fittings to achieve stable delivery of ligands and metal ionic liquids through laminar flow rather than turbulent flow. The laminar flow in microchannels contributes to controlling the speed of the reaction and reduce the aggregation of particles during biomimetic mineralization. The laminar flow is caused by the low Reynolds number determined by the hydraulic diameter of the channel, the flow rate, and the kinetic viscosity of the solution.^{31–33} Unfortunately, low Reynolds numbers in microfluidic devices greatly affect the mixing and reaction of the components.^{31–33} To address this challenge, various mixing enhancement methods have been explored to improve performance by changing the geometry and pattern in microfluidic devices, altering the properties of the channel surface.^{31,32} We designed and manufactured a specially structured receiver to extend the length of the tube and increase the reaction area. There were grooves on the inside of the cylindrical receiver that allowed the PTFE tubes to be placed spirally. The radius of the spiral was 45 mm, and the spacing of the spiral was 10 mm. In addition, ultrasonic oscillation can also promote adequate reaction.^{31,32} The oscillating bubbles produced by acoustic cavitation cause local turbulence that greatly alters the flow field; this enhances mass contact with each other and promotes passive reactions.³⁴ The ultrasound probe was placed at the center of the spiral PTFE tubes, which meant that the ultrasound probe was at a consistent distance from the PTFE tubes, so that the ultrasound oscillation received in the PTFE tubes during the

reaction was kept at a constant power. We utilized ultrasonic shock to facilitate the reaction and tested some parameters to obtain the optimal parameters for promoting the bionic mineralization of bacteria (Table S1).

3.2. Characterization of *Escherichia coli*@ZIF-8. *E. coli* is a common Gram-negative bacterium with various proteins on its cell wall and cell membrane.³⁵ Chen et al. proposed to use proteins to perform as prenuclear clusters on the reaction of ligands and metal ions.³⁶ Accordingly, we hypothesized that *E. coli* could also act as prenuclear clusters. To analyze whether ZIF-8 was formed on the surface of bacteria, a series of characterizations was made to encapsulated *E. coli*. The composition of encapsulated *E. coli* was detected by XPS, monitoring a wide binding energy region (0–1200 eV), encompassing the Zn 2p, O 1s, N 1s, and C 1s regions (Figure 1a). All expected ZIF-8 features were detected, including zinc (coordinating metal), nitrogen, and carbon (imidazole linker). The probe depth for XPS was approximately the top 20 atomic layers (~ 10 nm), so the collected XPS signals were from the surface of the encapsulated *E. coli*. To obtain more chemical information on the surface of encapsulated *E. coli*, the Zn 2p region was scanned with a higher resolution, which consists of two peaks (1019.7 and 1042.9 eV), as shown in Figure 1b.³⁷ The characteristic peaks in the X-ray diffraction pattern of *E. coli*@ZIF-8 at $2\theta = 8.24^{\circ}$, 13.64° , 17.36° , and 26.64° are in good agreement with those previously reported in the literature, as well as the synthesized and commercial ZIF-8.^{36,38} The XRD data confirmed that *E. coli*@ZIF-8 retained the same crystalline form as pure ZIF-8, indicating that the bacteria did not alter the crystalline structure of ZIF-8. To know whether *E. coli* cells have interactions with ZIF-8, we used Fourier transform infrared (FTIR) spectroscopy to characterize the interaction between ZIF-8 crystals and *E. coli* (Figure 1d). Some of the intense peaks ranging 400 to 700 cm^{-1} can be attributed to the stretching vibration of metal

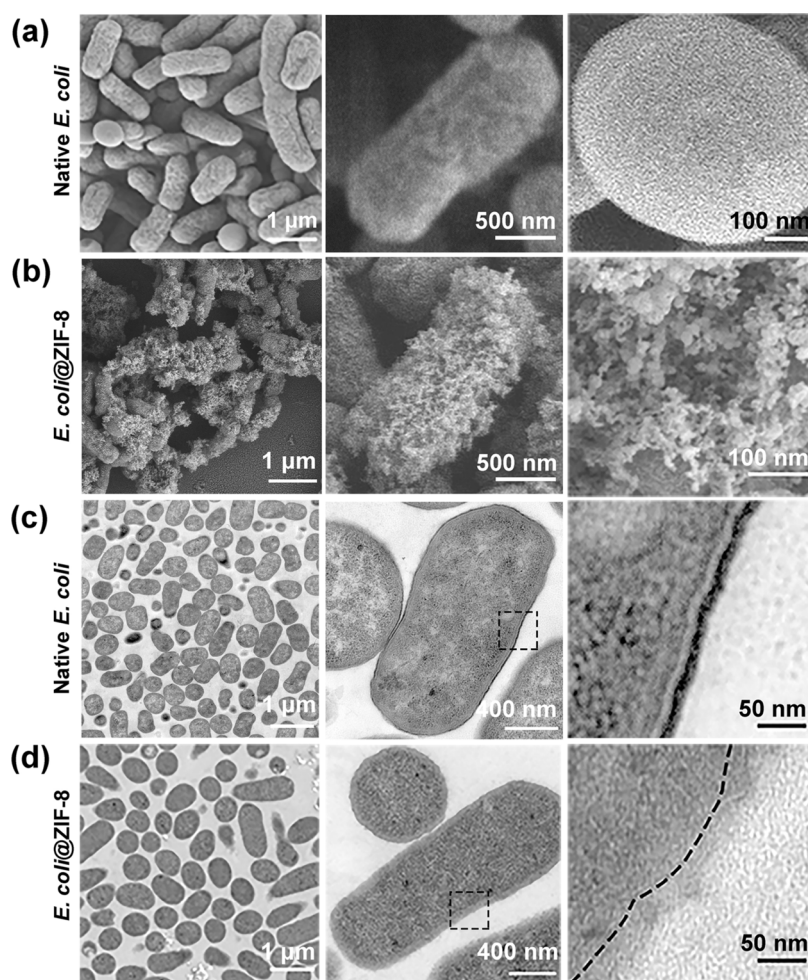


Figure 2. Morphological characterization of *Escherichia coli*@ZIF-8. SEM images of (a) native *E. coli* and (b) ZIF-8 coated *E. coli* were used as a control check. Low-magnification and high-magnification SEM photographs of the cells showing that the surface of the native *E. coli* (a) is smooth while the surface of the encapsulated *E. coli* (b) became rough. TEM images of (c) native *E. coli* and (d) ZIF-8 coated *E. coli*. (d) High-magnification TEM photographs of the encapsulated *E. coli* showed a continuous and uniform shell of approximately 20 nm.

oxide (Zn—O).³⁹ The energy band of 422 cm^{-1} of ZIF-8 and *E. coli*@ZIF-8 is attributed to the Zn—N bond. This absorption band reveals the vibrational properties of the Zn—N bond, which is apparently caused by the presence of ZIF-8 on the surface of *E. coli*. The bands of *E. coli*@ZIF-8 at 1424 and 1309 cm^{-1} are associated with asymmetric and symmetric vibrations of a C—H band, respectively.³⁹ Compared with the spectrum of native *E. coli*, the C—H band of *E. coli*@ZIF-8 is red-shifted from 1394 to 1377 cm^{-1} .³⁶ We can clearly observe in Figure S3 that, with the introduction of ZIF-8 into *E. coli*, the intensity of the peaks located at 1575 cm^{-1} decreased, which is related to the stretching vibration of C=N groups.³⁶ It can be proposed that hydrogen bonding occurs between the C=N bond of ZIF-8 and the hydroxyl group on the surface of *E. coli*, i.e., *E. coli*—OH...N=C-ZIF-8. The peak at 1654 cm^{-1} in *E. coli*@ZIF-8 corresponds to the asymmetric stretching vibrations of C=O in carboxylate groups.^{38,39} The broadband in the range $3000\text{--}3600\text{ cm}^{-1}$ corresponds to the O—H vibrations, which is different between *E. coli* and *E. coli*@ZIF-8.³⁸ It is proposed that the *E. coli* and ZIF-8 are bonded together *via* hydrogen bonding and the tendency of the positive zinc cations to the negative carboxylate group of the *E. coli*.^{39,40}

We assessed the ultrastructure and elemental distribution of *Escherichia coli*@ZIF-8. *E. coli* was rod-shaped with a length of about $2.0\text{ }\mu\text{m}$, and the diameters were around $0.25\text{--}1.0\text{ }\mu\text{m}$. The scanning electron microscopy (SEM) micrographs revealed that the surface of encapsulated cells become rough and uneven (Figure 2b) while the surface of naked cells was smooth (Figure 2a). Compared with the conventional method (Figure S1), we found that the microfluidic method reduced bacterial aggregations. The interconnection of encapsulated *E. coli* may be due to residues from the bionic mineralization process (Figure 2b).⁴¹ The ultrathin cross-section of *E. coli*@ZIF-8 was prepared by embedding the samples in epoxy resin. Then, the cross-section was observed under transmission electron microscopy (TEM) to investigate the interfacial boundary between ZIF-8 coating and *E. coli*. The encapsulated *E. coli* has an additional uniform shell of approximately 20 nm on the cell surface (Figure 2d) compared to the bare cells (Figure 2c). The elemental mapping indicated an uncannily similar distribution of Zn, C, O, and N on the cell surface, which strongly implied the formation of a homogeneous ZIF-8 coating on individual *E. coli* cells (Figure 3). The energy dispersive spectroscopy (EDS) spectrum indicates that the sample consists of carbon (0.277 keV), nitrogen (0.392 keV), and oxygen (0.525 keV) from bacteria (Figure S4). In

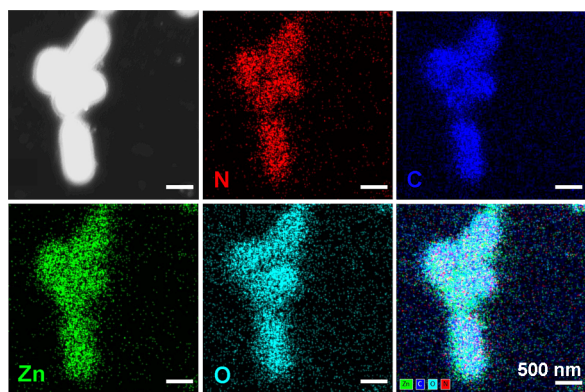


Figure 3. Mapping of the encapsulated cells in the TEM micrographs showed a high overlap in the distribution of N, C, Zn, and O. All samples were dried naturally.

addition, the zinc was detected at 1.0118 and 8.6313 keV.^{42,43} Figure S4 also listed the elemental analysis of *E. coli*@ZIF-8, with 16.9% of zinc, strongly indicating the presence of zinc in the encapsulated bacteria.

To verify the formation of a layer of MOF structure on the surface of *E. coli*, we performed qualitative experiments with laser confocal scanning microscopy and quantified it by flow cytometry. We used transgenic *E. coli* with a green fluorescent protein (Figure S5) and labeled ZIF-8 with red fluorescent rhodamine, excluding the effect of bacterial staining on colocalization results. It showed that the green fluorescent protein emitted by the bacteria largely overlapped with the red fluorescent position emitted by ZIF-8 (Figure 4a,b). Because

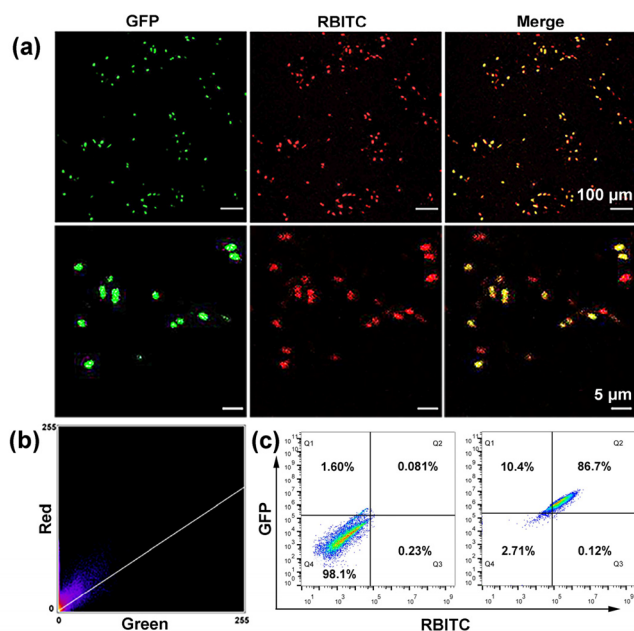


Figure 4. Colocalization of *Escherichia coli*@ZIF-8. (a) Confocal images of ZIF-8 coated transgenic *E. coli*, which could emit green fluorescence and the ZIF-8 coatings were labeled by Rhodamine B fluorescent dyes (red). (b) Colocalization analysis of confocal images (a) by Colocalization Finder of ImageJ, showing good colocalization of red and green fluorescence. (c) Results of flow cytometry of ZIF-8 coated transgenic *E. coli*. Transgenic *E. coli* can emit green fluorescence, and the ZIF-8 coatings were labeled by Rhodamine B fluorescent dyes (red).

of the small size of the bacteria, the red color of ZIF-8 largely overlapped with the whole bacterial body rather than only presented outside. The green and red fluorescence colocalized well after colocalization analysis by Colocalization Finder of ImageJ (Figure 4c), whose Pearson's correlation was 0.69 and indicated the significant correlation. The CLSM images and analysis results illustrated the successful synthesis of ZIF-8 outside the bacteria. There were 10.4% of bacteria that only emitted green fluorescence, indicating that transgenic *E. coli* were not encapsulated. Flow cytometry results showed that about 97.1% of transgenic *E. coli* emitted green fluorescence, with 86.7% of them emitting both green and red fluorescence, indicating that these bacteria were encapsulated by ZIF-8 (Figure 4d).

3.3. Tolerance of Encapsulated Bacteria to Harsh Environments. Subsequently, we centrifuged the original *E. coli* and the encapsulated *E. coli*, resuspended them in deionized water without nutrients, and left them separately at room temperature for 7 days. After resuspension of common bacteria in LB medium, there were almost no bacteria in the blank control group. The cell shell of the encapsulated bacteria was removed with EDTA to obtain a white mass (Figure S6a,b). Afterward, we also measured the production curves of the bacteria after removing the shell and the normal bacteria and found that the wrapped bacteria could recover their growth activity without any significant difference from the normal bacteria (Figure S6c). The protective effect of the cell shell on the cells was confirmed, allowing them to survive for longer periods in nutrient-deficient environments.

The process of wastewater treatment requires a combination of physical and chemical methods to complete water purification, of which UV irradiation is an important part.^{4,5,11} UV light, especially 254 nm, has long been known to exhibit antimicrobial effects,⁴⁴ so we expect the artificial bacterial shell to act as a physical barrier. After half an hour of UV irradiation, we removed the artificial shell of the bacteria and then incubated them for some time. Then, the bacterial viability was observed by live/dead cell staining. Surprisingly, most of the wrapped bacteria were still active after UV irradiation. The fluorescent microscopic images showed that the wrapped bacteria had more live bacteria and a few dead bacteria (Figure 5). As we known, the 254 nm light belongs to UVC, which is strong in energy but weak in penetration and is blocked by ordinary plastic and glass.⁴⁴ To investigate the principle of protection of bacteria by artificial shells, we examined the reactive oxygen species of natural and encapsulated bacteria with or without UV irradiation. The fluorescent probe DCFH-DA is not fluorescent and can freely pass through the cell membrane. After entering the cell, it can be hydrolyzed by intracellular esterases to generate DCF, which is not permeable to the cell membrane, thus allowing the probe to be easily loaded into the cell. The level of reactive oxygen species in the cell can be detected by detecting the fluorescence of DCF, which can be oxidized to produce fluorescent DCF. The stronger the green fluorescence signal indicates that reactive oxygen species (ROS) are more abundant. The fluorescence images showed that the natural cells produced a lot of reactive oxygen species after UV irradiation (Figure 6b) and the cell shell did not cause the cells to produce ROS (Figure 6c). Considering that the artificial cell shell may interfere with the entry of the fluorescent probe DCFH-DA into the cells, we irradiated the encapsulated cells with UV and then removed the shell and labeled the cells with

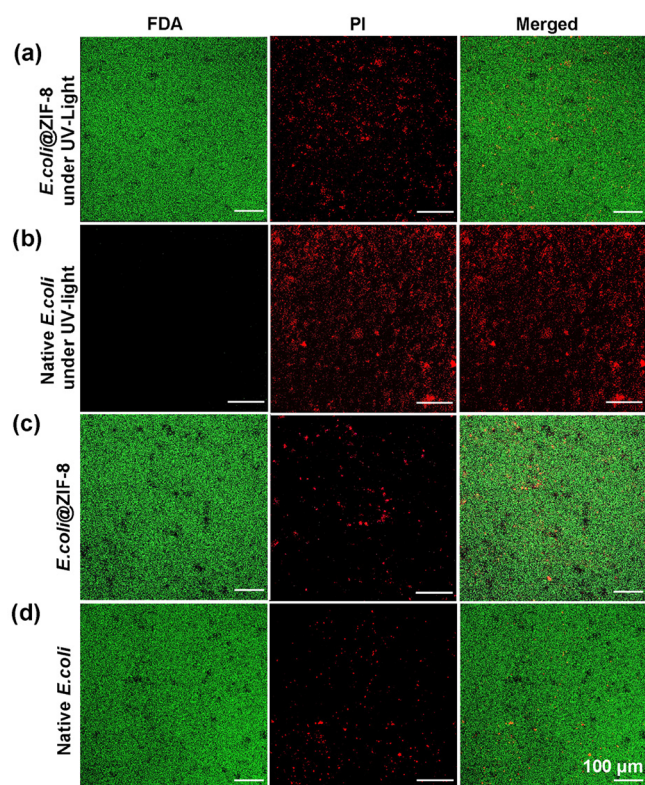


Figure 5. Resistance of bacteria with artificial shells to UV light. (a) ZIF-8-encapsulated *E. coli* after 30 min of irradiation with UV, (b) normal *E. coli* after 30 min of irradiation with UV, (c) ZIF-8-encapsulated *E. coli* without any treatment, and (d) untreated native *E. coli*. Live bacteria are labeled with FDA (green), and dead bacteria are labeled with PI (red).

the fluorescent probe DCFH-DA. After UV irradiation, the wrapped cells do not produce reactive oxygen species (Figure 6a). The quantified results of the fluorescence intensity showed that the production of intracellular ROS was greatly reduced after UV irradiation when the bacteria were wrapped (Figure 6e). The increased resistance of *E. coli* to UV light after wrapping was associated with a reduction in intracellular ROS.

To investigate whether the resistance of the bacteria to Cr(VI) was changed after the cells were wrapped, we suspended encapsulated and unencapsulated bacteria in an

aqueous solution containing 5 mg/L Cr (VI) and placed them on a shaker for 3 h. We obtained bacterial precipitates by centrifugation and removed the cell shells with EDTA. The bacteria were cultured in LB medium for a while, and live/dead cell staining was performed. It was found that a solution of 5 mg/L Cr (VI) caused most of the bare bacteria to be inactive with red fluorescence (Figure 7). In contrast, *E. coli* possessing

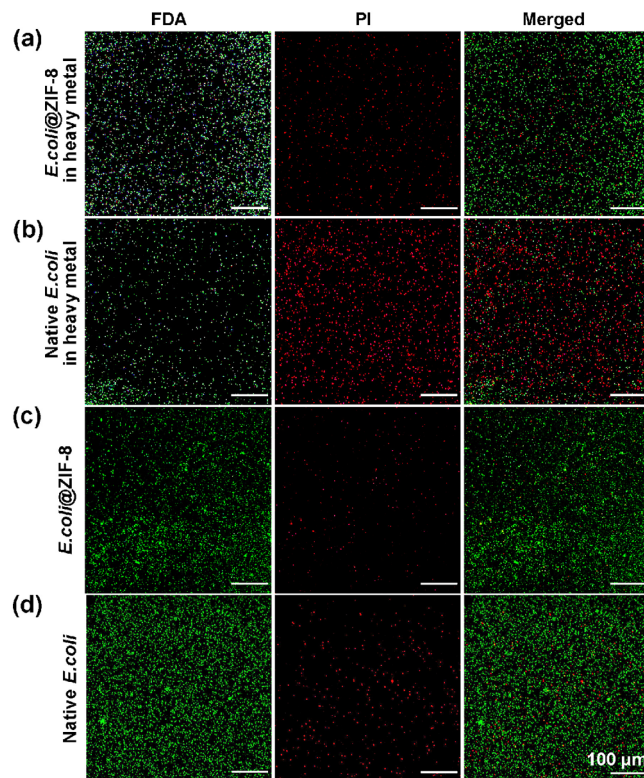


Figure 7. Resistance to hexavalent chromium of bacteria with artificial shells. (a) ZIF-8-encapsulated *E. coli* treated with 5 mg/L Cr (VI) solution, (b) normal *E. coli* treated with 5 mg/L Cr (VI) solution, (c) ZIF-8-encapsulated *E. coli* without any treatment, and (d) untreated native *E. coli*. Live bacteria are marked with FDA (green), and dead bacteria are marked with PI (red).

artificial cell shells treated with Cr (VI) solutions were mostly active with green fluorescence (Figure 7). The result of CLSM

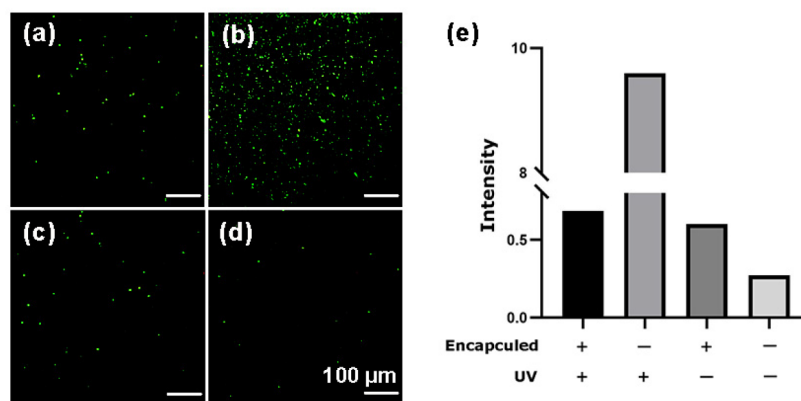


Figure 6. Reduction in ROS production by UV irradiation of bacteria with artificial shells. ROS are labeled with DCFH-DA (green): (a) ZIF-8-encapsulated *E. coli* after 30 min of irradiation with UV; (b) normal *E. coli* after 30 min of irradiation with UV; (c) ZIF-8-encapsulated *E. coli* without any treatment; (d) untreated native *E. coli*; and (e) the quantitative analysis of fluorescence intensity.

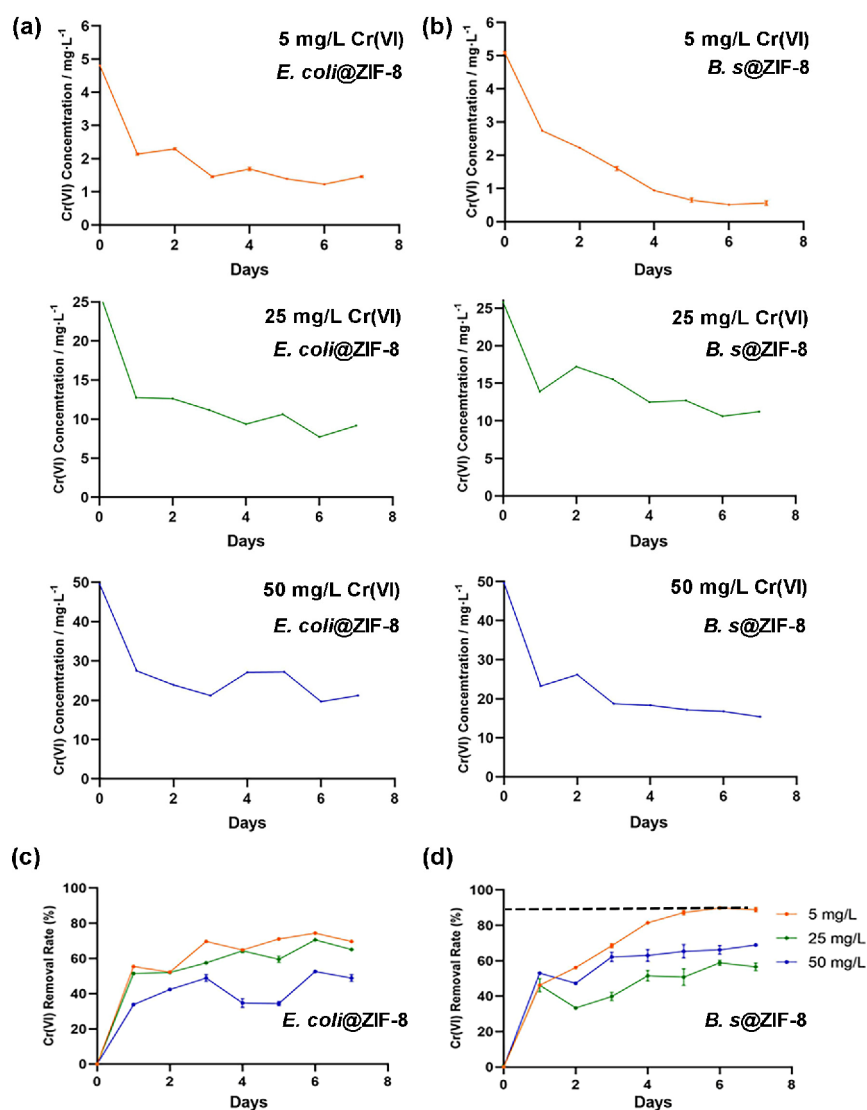


Figure 8. Concentration of hexavalent chromium in solution after treatment of (a) ZIF-8 encapsulated *E. coli* and (b) *Bacillus subtilis* with different concentrations of hexavalent chromium solution. (c) Removal rate of hexavalent chromium by encapsulated *E. coli* and (d) *Bacillus subtilis*.

indicated that the artificial cell shell increased the resistance of *E. coli* to Cr(VI) and acted as a cytoprotective agent. In the experiments above, we envisioned the use of a biomimetic mineralized shell to protect bacteria and improve their tolerance to heavy metals in contaminated water. It was confirmed that the artificial shell enhanced cellular tolerance to extreme environments, including nutrient deficiency, UV light, and heavy metal ions, which was limited for native bacterial cells.

3.4. Adsorption to Hexavalent Chromium of Bacteria with Artificial Shells. Bacterial remediation of chromium is fast, economical, environmentally friendly, and less energy intensive. Then, we tested the ability of native and encapsulated bacteria to adsorb heavy metals. We selected *E. coli* and *Bacillus subtilis* as Gram-positive and negative bacteria and representatives. It is worth mentioning that *Bacillus subtilis* is a probiotic bacteria, commonly found in soil and plant body surface, and also found in humans in the intestinal tract symbiotic *Bacillus subtilis*.¹⁶ Mass transport effects induced by the outer membrane of Gram-negative bacteria and the thin cell wall of peptidoglycan containing reductase promote the biosorption of heavy metals by Gram-negative bacteria.^{15,16} We

used the microfluidic method for the encapsulation of *E. coli* and *Bacillus subtilis*, treating aqueous solutions of 5, 25, and 50 mg/L hexavalent chromium. We found that 5 mg/L of hexavalent chromium was adsorbed at a higher rate than the others. It was inspiring that the uptake of hexavalent chromium could reach 90% by *Bacillus subtilis* after bionic mineralization when the concentration of hexavalent chromium was 5 mg/L (Figure 8d), compared with 74% for *E. coli* with an artificial shell (Figure 8c).

The removal rates of 25 mg/L Cr(VI) aqueous solution by encapsulated *E. coli* and *Bacillus subtilis* were 70% and 58%, respectively. When the concentration of hexavalent chromium was 50 mg/L, the uptake of hexavalent chromium by coated *E. coli* and *Bacillus subtilis* was 52% and 68%. Another interesting phenomenon is the rapid adsorption of Cr(VI) by bacteria possessing artificial ZIF-8 shells. For example, the biomaterialized *Bacillus subtilis* was used to treat 50 mg/L Cr(VI) in aqueous solutions; the concentration of Cr(VI) in the aqueous solution decreased to 23.3 mg/L after 1 day. The adsorption rate was as high as 53%, which was three-quarters of the final uptake rate. The adsorptions of 5, 25, and 50 mg/L hexavalent chromium by biomaterialized *E. coli* were 55%, 51%, and 33%

for the treatment of 1 day, respectively. Metal organic frameworks (MOFs) are rapidly entering the forefront of materials research due to their simple chemical tunability, impressive specific surface area, and selective adsorption power. The potential of deploying MOFs in water purification is related to the fact that their inner surface can be easily modified with a high density of strong adsorption sites during synthesis.^{26,28} As a result, there has been much interest in recent years in exploring inexpensive MOFs for water purification. Some studies have shown that the porous structure of ZIF-8 has a physical adsorption effect on heavy metals.^{26–28} To clarify the specific absorption mechanism, we tested the ability of ZIF-8, bacteria alone to absorb hexavalent chromium ions. The results confirmed that the uptake of Cr(VI) by ZIF-8 was faster and stabilized at 30% around after 2 days (Figure S7f). It is worth mentioning that ZIF-8 showed better absorption in a low concentration of hexavalent chromium solution, but the absorption rate in high concentration of hexavalent chromium solution was about the same as that of bacteria. The uptake of Cr(VI) by native *E. coli* was also faster in the first few days, stabilized at 31%, 14%, and 19% in the second day when the concentrations of hexavalent chromium were 5, 25, and 50 mg/L, respectively, and remained stable after that as well (Figure S7d). Similarly, the uptake of hexavalent chromium by *Bacillus subtilis* alone was relatively rapid during the first 3 days and remained stable thereafter. On the third day, when the concentrations were 5, 25, and 50 mg/L, the uptakes of hexavalent chromium were 39%, 20%, and 30% (Figure S7e). Therefore, we speculated that the early stage was dominated by physical adsorption and supplemented by biosorption. *E. coli* with an artificial shell was used to treat contaminated water containing 25 mg/L Cr(VI), and the Cr(VI) concentration in the aqueous solution decreased to 12.8 mg/L after a day (Figure 8a). On the following 4 days, the Cr(VI) concentrations in the aqueous solution remained stable, with concentrations at 12.6, 11.2, 9.4, and 10.6 mg/L, respectively. On the sixth day, the Cr(VI) concentration in the aqueous solution decreased again by 11.2% to 7.7 mg/L. We were very interested in this phenomenon and analyzed the other concentration groups and found that all showed another increase in uptake at a later stage, which remained stable later. In the *Bacillus subtilis* group, we found a similar situation. *Bacillus subtilis* possessing a super shell was used to treat Cr(VI) at 25 mg/L. After 1 day, the hexavalent chromium concentration decreased by 46% and remained essentially stable for the next 4 days (Figure 8d). On the sixth day, the absorption of hexavalent chromium reached its highest rate at around 60% and the concentration decreased to 10.6 mg/L (Figure 8d). Surprisingly, we found that the ZIF-8 encapsulated bacteria possessed a higher uptake rate than ZIF-8, bacteria alone at the initial stage. As we know, ZIF-8 is a porous material that has also been used in numerous studies for heavy metal uptake, but its uptake is limited.²⁸ In contrast, organisms, such as bacteria, can absorb some heavy metals, such as hexavalent chromium, through respiratory chain reactions and metabolic reactions associated with a variety of enzymes under conditions of heavy metal tolerance. In addition to biosorption, microorganisms can achieve bio-reduction of Cr(VI) with the same effect as the use of chemical reducing agents.¹⁶ A variety of microorganisms have been shown to be able to reduce Cr(VI) directly or indirectly, and their metabolites are also capable of acting as reducing agents, such as organic acids, amino acids, sulfides, and divalent

iron.^{2,15,16} Intracellular and membrane-bound Cr(VI) reduction is usually mediated by flavin-dependent reductase and hydrogenase, respectively, while extracellular and periplasmic Cr(VI) reduction is accomplished by cytochromes.² Intracellular reduction of Cr(VI) is the common pathway, and the influencing factors are NADH, flavin proteins, and other heme proteins. In the presence of oxygen, NADH and NADPH are electron donors while the associated reductase acts as an intermediate. In the absence of oxygen, Cr(VI) acts as a terminal electron acceptor in the respiratory chain and is also associated with proteins of the cytochrome family.¹² Bacteria first biosorb Cr(VI) and then translocate Cr(VI) into the cell *via* sulfate or phosphate channels. Cr(VI) is reduced by chromate reductase and the reduction product is translocated out of the cell *via* plasmids (Figure S8).¹⁶ The enzymatic reduction of Cr(VI) by *E. coli* is dependent on oxygen-insensitive NADPH nitroreductase, which was encoded by the *nfsA* gene.¹⁴ However, the different electron transfer mechanisms of these bacterial reductases need to be further investigated. When the heavy metals reach a certain concentration, the bacteria are unable to tolerate too high a concentration of heavy metals, and the bacteria gradually die and then decompose, turning into biomass. In this way, after bacterial lysis, the functional groups of various proteins are exposed and the absorption area is increased, which can improve the absorption of heavy metals again, so the encapsulated bacteria later showed a secondary increase in Cr(VI) uptake. We have shown that the ZIF-8 shell protects the bacteria in heavy metal solutions and may be one of the reasons for the secondary increase in uptake rate at a later stage. It suggests that our core–shell structure acts as a one plus one greater than two effect, improving the uptake of hexavalent chromium by ZIF-8 and bacteria. The encapsulation of bacteria increased not only the initial uptake rate of Cr(VI) but also the final uptake rate. Therefore, bacteria encapsulated with artificial shells kill two birds with one stone in treating heavy metal water contamination. Bacteria with ZIF-8 shells act as physical and biosorption first, followed by secondary biosorption after system decomposition. There is no doubt that our results provide a novel idea and approach to solve the water pollution problem. In the future, we will explore the specific mechanism of hexavalent chromium uptake by encapsulated bacteria in depth, which will eventually be used for the uptake of other heavy metal ions.

4. CONCLUSIONS

In summary, the composite of bacteria and other materials gives bacteria more functions, and bacteria with MOF shells have great potential in treating heavy metal ions in contaminated water. We used ZIF-8 to encapsulate the bacteria, SEM and TEM observations compared the bacteria before and after encapsulation, and it was observed that the encapsulated *E. coli* had a uniform and consistent shell on the surface. XRD characterization illustrated that the ZIF-8 shell of the bacteria was well-crystallized, and FTIR verified the existence of interactions between the bacteria and the ZIF-8 shell, such as covalent bonding, hydrogen bonding, etc. It was observed that bacteria and ZIF-8 colocalized well by CLSM and flow cytometry, with 86.7% of the wrapped bacteria. *In situ* formation of ZIF-8 on the cell surface completes the encapsulation of *E. coli*, improving the tolerance of bacteria to extreme environments such as nutrient deficiencies, UV light, and heavy metals. When the encapsulated *E. coli* was

placed in a nutrient-deficient environment after a week, the *E. coli* maintained the same activity as the original. The encapsulated bacteria could be used to absorb heavy metal ions, such as hexavalent chromium. *Bacillus subtilis* is a probiotic bacterium, and *Bacillus subtilis*@ ZIF-8 could absorb 90% of hexavalent chromium ions in aqueous solution. Another interesting phenomenon is the initial high absorption rate, which can absorb up to 50% of hexavalent chromium ions within 3 days, significantly higher than ZIF-8 and bacteria alone. With the passage of time, some metabolites of bacteria are acidic, ZIF-8 decomposes, the contact area between bacteria and heavy metal ions increases, and the absorption rate increases again. Therefore, the final uptake rate of hexavalent chromium by ZIF-8-encapsulated bacteria was higher than the uptake rate of bacteria and ZIF-8 alone. Our microfluidic device can gently encapsulate bacteria, granting them the ability to tolerate adverse environments and offering the possibility of future microbial applications in the environment and other fields.

■ ASSOCIATED CONTENT

SI Supporting Information

The Supporting Information is available free of charge at <https://pubs.acs.org/doi/10.1021/acsomega.1c06877>.

Figures of SEM images of encapsulated *E. coli* by the conventional method, microfluidic device, FTIR spectra of native *E. coli*, *E. coli*@ZIF-8, EDS of encapsulated *E. coli*, and pure ZIF-8, fluorescence micrographs of normal *E. coli* and transgenic *E. coli*, growth activity of encapsulated bacteria after 7 days of nutrient deficiency, concentration and removal rate of hexavalent chromium after treatment with *E. coli*, *Bacillus subtilis*, and ZIF-8, respectively, and mechanism of bacterial bioreduction of hexavalent chromium and table of optimization of ultrasound-related parameters (PDF)

■ AUTHOR INFORMATION

Corresponding Author

Jing Wang – School of Stomatology, Lanzhou University, Lanzhou, Gansu 730000, China; Clinical Research Center for Oral Diseases, Lanzhou, Gansu 730000, China; orcid.org/0000-0003-4481-0032; Email: lzuckwj@126.com

Authors

Rongbing Tang – School of Stomatology, Lanzhou University, Lanzhou, Gansu 730000, China; Clinical Research Center for Oral Diseases, Lanzhou, Gansu 730000, China

Liheng Shen – School of Stomatology, Lanzhou University, Lanzhou, Gansu 730000, China; Clinical Research Center for Oral Diseases, Lanzhou, Gansu 730000, China

Lu Yang – School of Stomatology, Lanzhou University, Lanzhou, Gansu 730000, China; Clinical Research Center for Oral Diseases, Lanzhou, Gansu 730000, China

Kai You – School of Stomatology, Lanzhou University, Lanzhou, Gansu 730000, China; Clinical Research Center for Oral Diseases, Lanzhou, Gansu 730000, China

Zhihui Li – School of Stomatology, Lanzhou University, Lanzhou, Gansu 730000, China; Clinical Research Center for Oral Diseases, Lanzhou, Gansu 730000, China

Xiaorui Wei – School of Stomatology, Lanzhou University, Lanzhou, Gansu 730000, China; Clinical Research Center for Oral Diseases, Lanzhou, Gansu 730000, China

Complete contact information is available at: <https://pubs.acs.org/doi/10.1021/acsomega.1c06877>

Author Contributions

[§]R.T. and L.S. contributed equally to this work. L.S., L.Y., K.Y., Z.L., and X.W. provided ideas and carried out all the experiments. R.T. and L.S. conceptualized projects, designed, and directed experiments. R.T. and J.W. conceived the project and supported the technology platform. R.T. and L.S. organized, wrote, and revised the paper. J.W. and L.Y. revised the paper. All authors discussed the results and analyzed the data.

Notes

The authors declare no competing financial interest.

■ ACKNOWLEDGMENTS

This work was supported by the National Natural Science Foundation of China (82101011), the Natural Science Foundation of Gansu Province (20YF8WA084, 20JR10FA670), and the Central University Basic Research Fund of China (lzujbky-2020-51), and School/Hospital of Stomatology, Lanzhou University (lzukqky-2019-y09) is also acknowledged with gratitude.

■ ABBREVIATIONS USED

MOFs, metal–organic frameworks; ZIF-8, zeolitic imidazolate framework-8; *E. coli*, *Escherichia coli*; *E. coli*@ZIF-8, *Escherichia coli*@zeolitic imidazolate framework-8; BSA-RBITC, Bull serum albumin-Rhodamine B isothiocyanate; ROS, reactive oxygen species; 2MI, 2-methylimidazole; CLSM, confocal laser scanning microscope; SEM, scanning electron microscope; TEM, transmission electron microscope; XRD, X-ray diffraction; XPS, X-ray photoelectron spectra; FTIR, Fourier transform infrared spectroscopy; EDS, energy dispersive spectroscopy; UV, ultraviolet; OD₆₀₀, optical density at 600 nm; FDA, fluorescein diacetate; PI, propidium iodide

■ REFERENCES

- (1) Saha, R.; Nandi, R.; Saha, B. Sources and toxicity of hexavalent chromium. *J. Coord. Chem.* **2011**, *64*, 1782–1806.
- (2) Jobby, R.; Jha, P.; Yadav, A. K.; Desai, N. Biosorption and biotransformation of hexavalent chromium Cr(VI): A comprehensive review. *Chemosphere* **2018**, *207*, 255–266.
- (3) Jiang, Y. T.; Yang, F.; Dai, M.; Ali, I.; Shen, X.; Hou, X. T.; Alhewairini, S. S.; Peng, C. S.; Naz, I. Application of microbial immobilization technology for remediation of Cr(VI) contamination: A review. *Chemosphere* **2022**, *286*, 131721.
- (4) Karimi-Maleh, H.; Ayati, A.; Ghanbari, S.; Orooji, Y.; Tanhaei, B.; Karimi, F.; Alizadeh, M.; Rouhi, J.; Fu, L.; Sillanpaa, M. Recent advances in removal techniques of Cr(VI) toxic ion from aqueous solution: A comprehensive review. *J. Mol. Liq.* **2021**, *329*, 115062.
- (5) Barrera-Diaz, C. E.; Lugo-Lugo, V.; Bilyeu, B. A review of chemical, electrochemical and biological methods for aqueous Cr(VI) reduction. *J. Hazard. Mater.* **2012**, *223*, 1–12.
- (6) Zhao, Z. Y.; An, H.; Lin, J.; Feng, M. C.; Murugadoss, V.; Ding, T.; Liu, H.; Shao, Q.; Mai, X. M.; Wang, N.; Gu, H. B.; Angaiah, S.; Guo, Z. H. Progress on the Photocatalytic Reduction Removal of Chromium Contamination. *Chem. Rec.* **2019**, *19*, 873–882.
- (7) Saleh, T. A. Trends in the sample preparation and analysis of nanomaterials as environmental contaminants. *Trends in Environmental Analytical Chemistry* **2020**, *28*, No. e00101.

- (8) Saleh, T. A. *Characterization, determination and elimination technologies for sulfur from petroleum: Toward cleaner fuel and a safe environment. Trends in Environmental Analytical Chemistry* **2020**, *25*, No. e00080.
- (9) Saleh, T. A. Nanomaterials: Classification, properties, and environmental toxicities. *Environmental Technology & Innovation* **2020**, *20*, 101067.
- (10) Saleh, T. A. Protocols for synthesis of nanomaterials, polymers, and green materials as adsorbents for water treatment technologies. *Environmental Technology & Innovation* **2021**, *24*, 101821.
- (11) GracePavithra, K.; Jaikumar, V.; Kumar, P. S.; SundarRajan, P. A review on cleaner strategies for chromium industrial wastewater: Present research and future perspective. *J. Clean Prod.* **2019**, *228*, 580–593.
- (12) Xia, S. P.; Song, Z. L.; Jeyakumar, P.; Shaheen, S. M.; Rinklebe, J.; Ok, Y. S.; Bolan, N.; Wang, H. L. A critical review on bioremediation technologies for Cr(VI)-contaminated soils and wastewater. *Crit. Rev. Environ. Sci. Technol.* **2019**, *49*, 1027–1078.
- (13) Singh, P.; Itankar, N.; Patil, Y. Biomangement of hexavalent chromium: Current trends and promising perspectives. *J. Environ. Manage.* **2021**, *279*, 111547.
- (14) Xia, X.; Wu, S. J.; Zhou, Z. J.; Wang, G. J. Microbial Cd(II) and Cr(VI) resistance mechanisms and application in bioremediation. *J. Hazard. Mater.* **2021**, *401*, 123685.
- (15) Chen, J.; Tian, Y. Q. Hexavalent chromium reducing bacteria: mechanism of reduction and characteristics. *Environ. Sci. Pollut. Res.* **2021**, *28*, 20981–20997.
- (16) Ahmad, W. A.; Venil, C. K.; Chirwa, E. M. N.; Wang, Y. T.; Sani, M. H.; Samad, A. F. A.; Kamaruddin, M. F. A.; Donati, E. R.; Urbietta, M. S.; Zakaria, Z. A. Bacterial Reduction of Cr(VI): Operational Challenges and Feasibility. *Curr. Pollut. Rep.* **2021**, *7*, 115–127.
- (17) Li, J. Y.; Tang, C.; Zhang, M.; Fan, C.; Guo, D. B.; An, Q. Y.; Wang, G. S.; Xu, H.; Li, Y.; Zhang, W.; Chen, X. X.; Zhao, R. Exploring the Cr(VI) removal mechanism of *Sporosarcina saromensis* M52 from a genomic perspective. *Ecotox. Environ. Safe.* **2021**, *225*, 112767.
- (18) Zhu, W.; Guo, J. M.; Amini, S.; Ju, Y.; Agola, J. O.; Zimpel, A.; Shang, J.; Noureddine, A.; Caruso, F.; Wuttke, S.; Croissant, J. G.; Brinker, C. J. SupraCells: Living Mammalian Cells Protected within Functional Modular Nanoparticle-Based Exoskeletons. *Adv. Mater.* **2019**, *31*, 1900545.
- (19) Youn, W.; Kim, J. Y.; Park, J.; Kim, N.; Choi, H.; Cho, H.; Choi, I. S. Single-Cell Nanoencapsulation: From Passive to Active Shells. *Adv. Mater.* **2020**, *32*, 1907001.
- (20) Chong, L. S. H.; Zhang, J. Y.; Bhat, K. S.; Yong, D.; Song, J. Bioinspired cell-in-shell systems in biomedical engineering and beyond: Comparative overview and prospects. *Biomaterials* **2021**, *266*, 120473.
- (21) Griesshaber, E.; Schmahl, W. Special Issue on Biomineralization: From Cells to Biomaterials. *Acta Biomater.* **2021**, *120*, 1–3.
- (22) Zhao, Y. Q.; Tang, R. K. Improvement of organisms by biomimetic mineralization: A material incorporation strategy for biological modification. *Acta Biomater.* **2021**, *120*, 57–80.
- (23) Ha, L.; Ryu, U.; Kang, D. C.; Kim, J. K.; Sun, D.; Kwon, Y. E.; Choi, K. M.; Kim, D. P. Rapid Single-Step Growth of MOF Exoskeleton on Mammalian Cells for Enhanced Cytoprotection. *ACS Biomater. Sci. Eng.* **2021**, *7*, 3075–3081.
- (24) Liang, J. Y.; Liang, K. Nano-bio-interface engineering of metal-organic frameworks. *Nano Today* **2021**, *40*, 101256.
- (25) Velasquez-Hernandez, M. D.; Linares-Moreau, M.; Astria, E.; Carraro, F.; Alyami, M. Z.; Khashab, N. M.; Sumbly, C. J.; Doonan, C. J.; Falcaro, P. Towards applications of bioentities@MOFs in biomedicine. *Coord. Chem. Rev.* **2021**, *429*, 213651.
- (26) Rojas, S.; Horcajada, P. Metal-Organic Frameworks for the Removal of Emerging Organic Contaminants in Water. *Chem. Rev.* **2020**, *120*, 8378–8415.
- (27) Shellaiah, M.; Sun, K. W. Progress in Metal-Organic Frameworks Facilitated Mercury Detection and Removal. *Chemosensors* **2021**, *9*, 101.
- (28) Duan, C. X.; Yu, Y.; Xiao, J.; Li, Y. Y.; Yang, P. F.; Hu, F.; Xi, H. X. Recent advancements in metal-organic frameworks for green applications. *Green Energy Environ.* **2021**, *6*, 33–49.
- (29) Liang, K.; Richardson, J. J.; Cui, J. W.; Caruso, F.; Doonan, C. J.; Falcaro, P. Metal-Organic Framework Coatings as Cytoprotective Exoskeletons for Living Cells. *Adv. Mater.* **2016**, *28*, 7910–7914.
- (30) Singhvi, M. S.; Zinjarde, S. S.; Gokhale, D. V. Polylactic acid: synthesis and biomedical applications. *J. Appl. Microbiol.* **2019**, *127*, 1612–1626.
- (31) Ward, K.; Fan, Z. H. Mixing in microfluidic devices and enhancement methods. *J. Micromech. Microeng.* **2015**, *25*, 094001.
- (32) Lee, C. Y.; Wang, W. T.; Liu, C. C.; Fu, L. M. Passive mixers in microfluidic systems: A review. *Chem. Eng. J.* **2016**, *288*, 146–160.
- (33) Lee, C. Y.; Chang, C. L.; Wang, Y. N.; Fu, L. M. Microfluidic Mixing: A Review. *Int. J. Mol. Sci.* **2011**, *12*, 3263–3287.
- (34) Zhao, S. N.; Yao, C. Q.; Dong, Z. Y.; Chen, G. W.; Yuan, Q. Role of ultrasonic oscillation in chemical processes in microreactors: A mesoscale issue. *Particuology*, **2020**, *48*, 88–99.
- (35) Sleytr, U. B.; Schuster, B.; Egelseer, E. M.; Pum, D. S-layers: principles and applications. *F Microbiol. Rev.* **2014**, *38*, 823–864.
- (36) Chen, T. T.; Yi, J. T.; Zhao, Y. Y.; Chu, X. Biomineralized Metal-Organic Framework Nanoparticles Enable Intracellular Delivery and Endo-Lysosomal Release of Native Active Proteins. *J. Am. Chem. Soc.* **2018**, *140*, 9912–9920.
- (37) Tian, F. Y.; Cerro, A. M.; Mosier, A. M.; Wayment-Steele, H. K.; Shine, R. S.; Park, A.; Webster, E. R.; Johnson, L. E.; Johal, M. S.; Benz, L. Surface and Stability Characterization of a Nanoporous ZIF-8 Thin Film. *J. Phys. Chem. C* **2014**, *118*, 14449–14456.
- (38) Vahed, T. A.; Naimi-Jamal, M. R.; Panahi, L. Alginate-coated ZIF-8 metal-organic framework as a green and bioactive platform for controlled drug release. *J. Drug Delivery Sci. Technol.* **2019**, *49*, 570–576.
- (39) Saleh, T. A. Simultaneous adsorptive desulfurization of diesel fuel over bimetallic nanoparticles loaded on activated carbon. *J. Clean Prod.* **2018**, *172*, 2123–2132.
- (40) Saleh, T. A. Nanocomposite of carbon nanotubes/silica nanoparticles and their use for adsorption of Pb(II): from surface properties to sorption mechanism. *Desalination and Water Treatment* **2016**, *57*, 10730–10744.
- (41) Adio, S. O.; Omar, M. H.; Asif, M.; Saleh, T. A. Arsenic and selenium removal from water using biosynthesized nanoscale zero-valent iron: a factorial design analysis. *Process Safety and Environmental Protection* **2017**, *107*, 518–527.
- (42) Saleh, T. A.; Tuzen, M.; Sari, A.; et al. Polyethylenimine modified activated carbon as novel magnetic adsorbent for the removal of uranium from aqueous solution. *Chem. Eng. Res. Des.* **2017**, *117*, 218–227.
- (43) Saleh, T. A.; Tuzen, M.; Sari, A. Polyamide magnetic palygorskite for the simultaneous removal of Hg (II) and methyl mercury; with factorial design analysis. *J. Environ. Manage.* **2018**, *211*, 323–333.
- (44) Rezaie, A.; Leite, G. G. S.; Melmed, G. Y.; Mathur, R.; Villanueva-Millan, M. J.; Parodi, G.; Sin, J.; Germano, J. F.; Morales, W.; Weitsman, S.; Kim, S. Y.; Park, J. H.; Sakhaie, S.; Pimentel, M. Ultraviolet a light effectively reduces bacteria and viruses including coronavirus. *PLoS one*, **2020**, *15*, No. e0236199.